

Supplement of

The role of atmospheric rivers in the distribution of heavy precipitation events over North America

Sara M. Vallejo-Bernal et al.

Correspondence: Sara M. Vallejo-Bernal (vallejo.bernal@pik-potsdam.de)

S1 Spatial pattern of heavy precipitation events (HPEs) in North America (NA)

To illustrate the ERA5 precipitation estimates used for our analysis, in fig S1 we show the spatial pattern of HPEs in NA, obtained by thresholding the daily precipitation estimates at the 95-th percentile. Only days exceeding 1 mm of total precipitation were used for computing the percentiles. Specially note that the highest values of the 95-th percentile are along the western coast of NA, where the topography plays a crucial role in the land-falling of ARs and where the most intense HPEs occur.

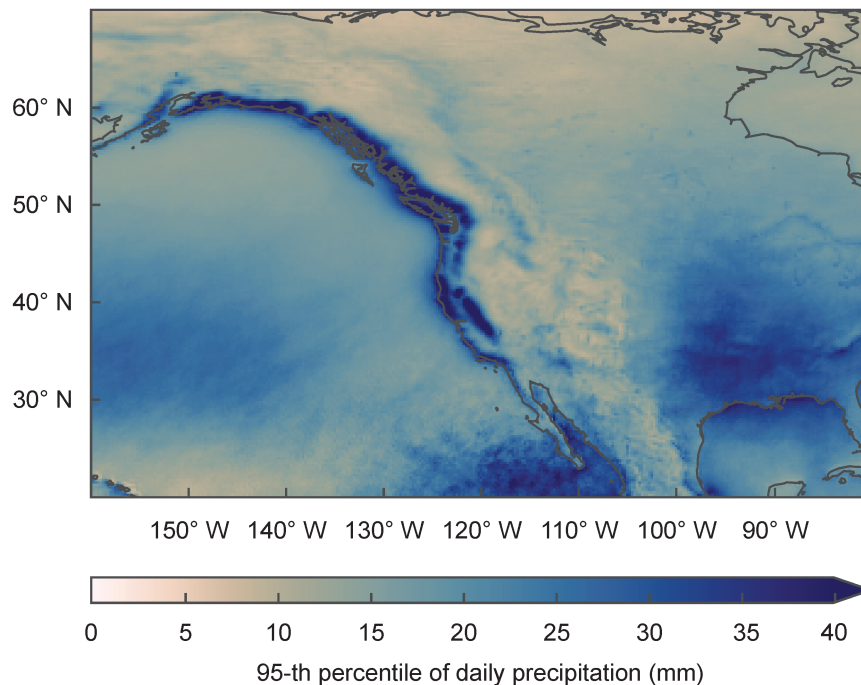


Figure S1. 95-th percentile thresholds of precipitation considering only wet days (days exceeding 1 mm of total precipitation).

S2 Analysis of the impact of latitudinally categorized atmospheric rivers (ARs).

In the main manuscript, we have only used ARs making landfall north of 47.5° . We based that on the finding that the number of grid cells at which HPEs are significantly correlated with ARs is not increased by including ARs making landfall at lower latitudes. For that, we have step-wise included more ARs (with a 2.5° step size) and counted the number of significant grid cells in central and eastern Canada (for the spatial extent, see red box in Fig. 5b). As an illustration of how the results appear when including all ARs, we have run the analysis evaluating the synchronization between HPEs and ARs making landfall anywhere on the western coast of NA. We show Fig. S2, featuring otherwise the same key findings as in Fig. 2.

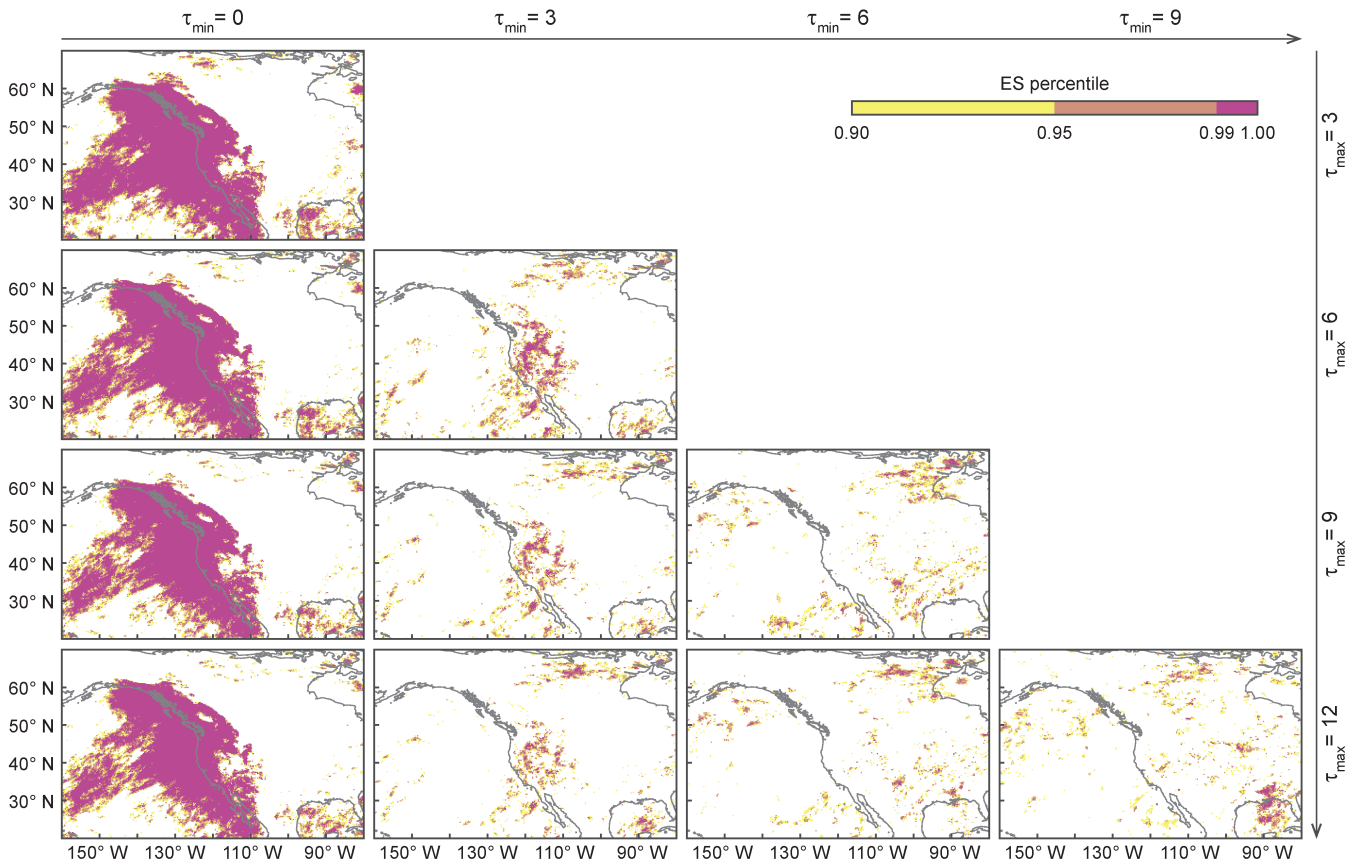


Figure S2. Event synchronization (ES) between ARs making landfall on the western coast of NA and HPEs. We use the SIO-R1 catalog of land-falling ARs and consider all ARs of level AR3 or higher. Different values of τ_{\min} and τ_{\max} are considered to calculate ES in each panel: τ_{\min} increases from left to right and τ_{\max} from top to bottom. Color bar as in Fig. 2.

As the results shown in Fig. 2 and Fig. S2 are not visually distinguishable in central and eastern Canada and the number of grid cells exhibiting significant synchronization does not increase in that region, we assume our choice is robust and proceeded with the subset of ARs for the main analysis.

S3 Dependence on the choice of the AR catalog

As mentioned in the introduction, a plethora of work has analyzed how the choice of an AR detection algorithm affects the outcome of an analysis (Shields et al., 2018; Rutz et al., 2019; O’Brien et al., 2022). For this reason, we have re-run the whole analysis for a systematically different AR catalog (for details see Sec. 2). Whereas in the main manuscript we utilized the SIO-
 20 R1 catalog by Gershunov et al. (2017), here we feature the analysis carried out with a catalog based on the IPART algorithm (Xu et al., 2020; Traxl, 2022).

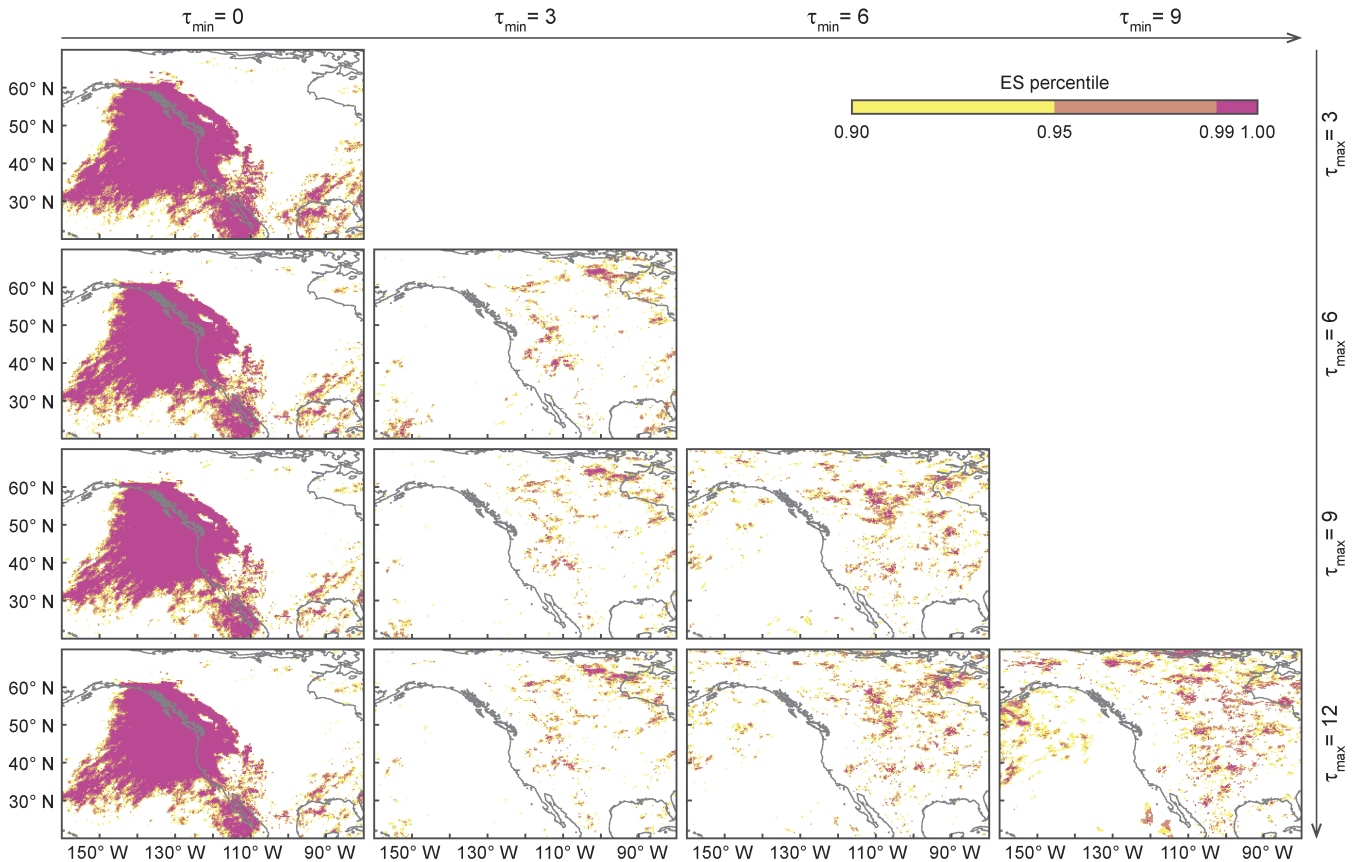


Figure S3. Event synchronization (ES) between ARs making landfall on the western coast of NA and HPEs. We use the IPART catalog of land-falling ARs and consider all ARs of level AR2 or higher. Different values of τ_{\min} and τ_{\max} were considered to calculate ES in each panel: τ_{\min} increases from left to right and τ_{\max} from top to bottom. Color bar as in Fig. 2.

To verify that we find, in principle, the same results using this alternative approach, we again show the results of assessing the synchronization between land-falling ARs and HPEs, and as in the previous section, we consider all ARs making landfall anywhere on the western coast of NA. The results are shown in Fig. S3 and, as expected, are visibly different to some extent,
 25 so we must acknowledge that we had to adapt the parameters of the analysis. In particular, for the IPART catalog, we reduced

the considered lower threshold for the AR level. Therefore, Fig. S3 is based on ARs of level AR2 and higher, whereas Fig. S2, and Fig. 2 are based on ARs of level AR3 and higher. We assume that this is due to two reasons: first, ARs identified by the IPART catalog have, on average, a shorter persistence in comparison to the ones listed in the SIO-R1 catalog. Therefore, ARs are often ranked higher in the SIO-R1 catalog (persistence is one criterion on the AR scale by Ralph et al., 2019). Second, the IPART algorithm identified significantly fewer ARs, which leads to a more sparse AR time series. Then, filtering out many ARs may decrease the ES score due to the sparsity of the time series.

Aside from this adaptation, which we consider reasonable, we again find a region of synchronization between land-falling ARs and HPEs in central and eastern Canada. Note that the results show striking qualitative similarity (the signal is strongest for $\tau_{\min} \geq 3$ and $\tau_{\max} = 12$), and for $\tau_{\min} \geq 3$ the signal close to the coast vanishes/gets less significant). Therefore, we consider the results based on the IPART catalog (Fig. S3) comparable to the results featured in the main manuscript (Fig. 2).

To be transparent regarding the construction of the IPART catalog we refer to Xu et al. (2020) and the chosen parameters below, which are mostly the default parameters of the algorithm.

Table S1. Parameters used to create the IPART AR catalog.

Parameter name	Short description of the parameter	Parameter value	Unit	Step of the IPART algorithm
kernel	List of integers specifying the shape of the structuring element used in the gray erosion process	[16, 6, 6]	-	Top-hat by Reconstruction computation on IVT data
shift_lon	Shifts data along longitude dimension	80	degrees longitude	Top-hat by Reconstruction computation on IVT data
thres_low	Define AR candidates as regions \geq this anomalous IVT	1	$kgm - 1_s - 1$	Detect AR appearances from Top-hat by Reconstruction output
min_area	Drop AR candidates smaller than this area	500.000	km^2	Detect AR appearances from Top-hat by Reconstruction output
max_area	Drop AR candidates larger than this area	18.000.000	km^2	Detect AR appearances from Top-hat by Reconstruction output
min_LW	Minimal length to width ratio	2	-	Detect AR appearances from Top-hat by Reconstruction output
min_lat	Exclude ARs whose centroids are lower than this latitude	20	degrees latitude	Detect AR appearances from Top-hat by Reconstruction output
max_lat	Exclude ARs whose centroids are higher than this latitude	80	degrees latitude	Detect AR appearances from Top-hat by Reconstruction output
min_length	ARs shorter than this length are treated as relaxed	2.000	km	Detect AR appearances from Top-hat by Reconstruction output
min_length_hard	ARs shorter than this length are discarded	1.500	km	Detect AR appearances from Top-hat by Reconstruction output
rip_thres	Error when simplifying axis using rip algorithm	2	degrees latitude/longitude	Detect AR appearances from Top-hat by Reconstruction output
fill_radius	Number of grids as radius to fill small holes in AR contour	4	-	Detect AR appearances from Top-hat by Reconstruction output
single_dome	Do peak partition or not, used to separate systems that are merged together with an outer contour	False	-	Detect AR appearances from Top-hat by Reconstruction output
edge_eps	Minimal proportion of flux component in a direction to total flux to allow edge building in that direction	0.4	-	Detect AR appearances from Top-hat by Reconstruction output
zonal_cyclic	Whether to treat the data as zonally cyclic	True	-	Detect AR appearances from Top-hat by Reconstruction output
TIME_GAP_ALLOW	Gap allowed to link 2 ARs	6	hours	Track ARs at individual time steps to form tracks
TRACK_SCHEME	Tracking scheme	simple	-	Track ARs at individual time steps to form tracks
MAX_DIST_ALLOW	Maximal Hausdorff distance to define a neighborhood relationship	1200	km	Track ARs at individual time steps to form tracks
MIN_DURATION	Minimal duration to keep a track	0	hours	Track ARs at individual time steps to form tracks
MIN_NONRELAX	Minimal number of non-relaxed records in a track to keep a track.	0	-	Track ARs at individual time steps to form tracks

S4 Dependence on the choice of the AR level

In the main manuscript we have stated that the synchronization pattern observed in the western coast of NA between land-falling ARs and HPEs occurring between 0 and 3 after the landfall does not change if ARs of the lower levels AR1 and AR2 are excluded from the calculations. This statement is based on the results shown in Fig. S4, which displays the grid points whose time series of HPEs are significantly synchronized with the AR time series, when $\tau_{\min} = 0$ and $\tau_{\max} = 3$. In panel (a) all the ARs are considered, and for the subsequent panels, ARs of the lower levels are step-wise excluded such that the lower limit of the considered AR level increases. Note that the most prominent synchronization pattern is always present along the western coast of NA, which is expected given the direct impact of ARs in the immediate HPEs of this area (Neiman et al., 2008; Gershunov et al., 2017; Waliser and Guan, 2017; Ralph et al., 2019). However, excluding ARs of the lower levels AR1 and AR2 does not change this result, as only considering ARs from levels AR4 and AR5 does. Including ARs of the lower levels for the calculations of ES introduces noise into the results, especially in eastern NA, where the synchronization pattern is not related to ARs making landfall on the West Coast but rather to ARs and extra-tropical cyclones making landfall on the East Coast. On the other hand, only considering ARs of levels AR4 and AR5 reduces the number of events and makes the AR time

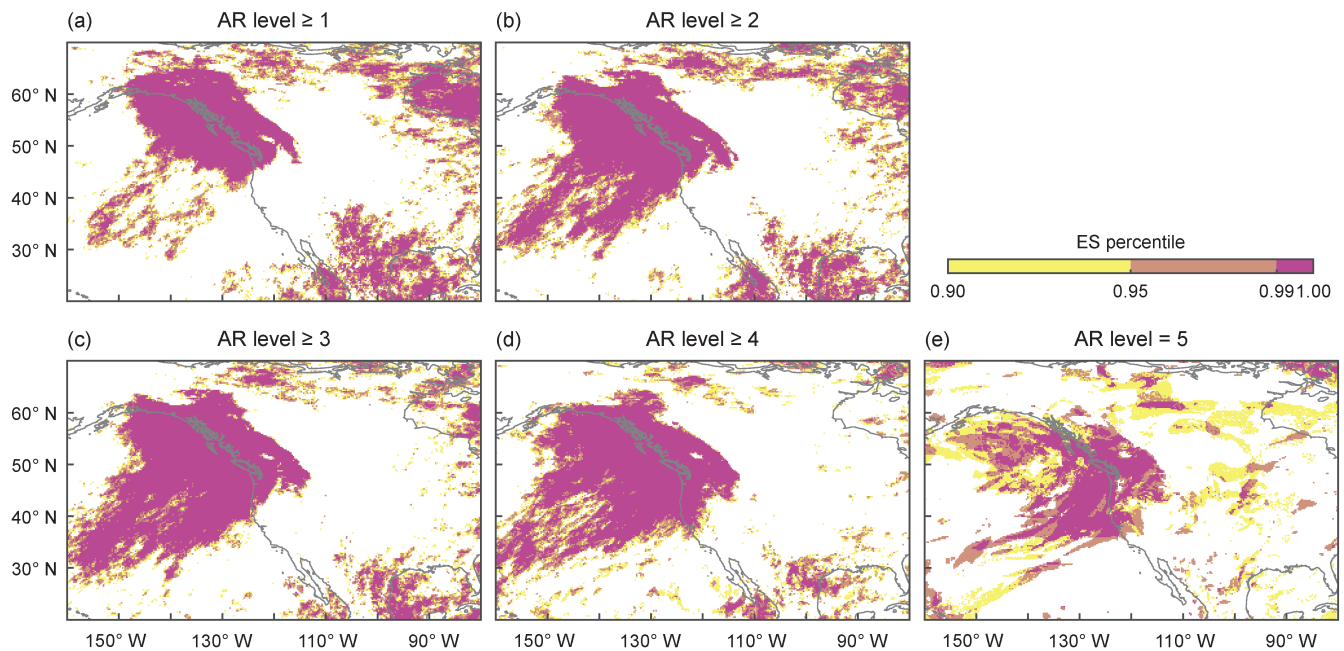


Figure S4. Event synchronization (ES) between ARs making landfall on the western coast of NA and HPEs. We use the SIO-R1 catalog of land-falling ARs but only consider ARs making landfall north of 47.5°N. ES is calculated with $\tau_{\min} = 0$ and $\tau_{\max} = 3$. From (a) to (e) the lower limit of the considered AR level increases: (a) ARs of level AR1 and higher e.g. all ARs, (b) ARs of level AR2 and higher, rest accordingly. Color bar as in Fig. 2.

series too sparse to retain the statistical significance of the results. Since panel (c) exhibits an intermediate pattern between these 2 scenarios, we have selected ARs of level AR3 or higher for our analysis.

S5 Synoptic conditions during type II and III events

In the main manuscript we revealed the synoptic conditions facilitating the delayed effect of ARs in the precipitation over central and eastern Canada. We did so by analyzing composite anomalies of IVT, geopotential height at 500 hPa, wind at 500 hPa, and precipitation, on the days of type I events (when the highly synchronized ARs made landfall) and for the following 3, 5, and 12 days. Now, we contrast those results with the composite analysis for type II and III events, i.e. for days after the landfall of ARs that did not synchronize with HPEs in central and eastern Canada, and for days before HPEs in central and eastern Canada that occurred in the absence of a land-falling AR (see Sec. 3.5 for a detailed description of the types of events).

In Fig. S5, we first present temporal evolution of the synoptic conditions after the landfall of ARs that did not synchronize with HPEs in central and eastern Canada. As in Fig. 7, when lag = 0 days, there is a high positive IVT anomaly on the

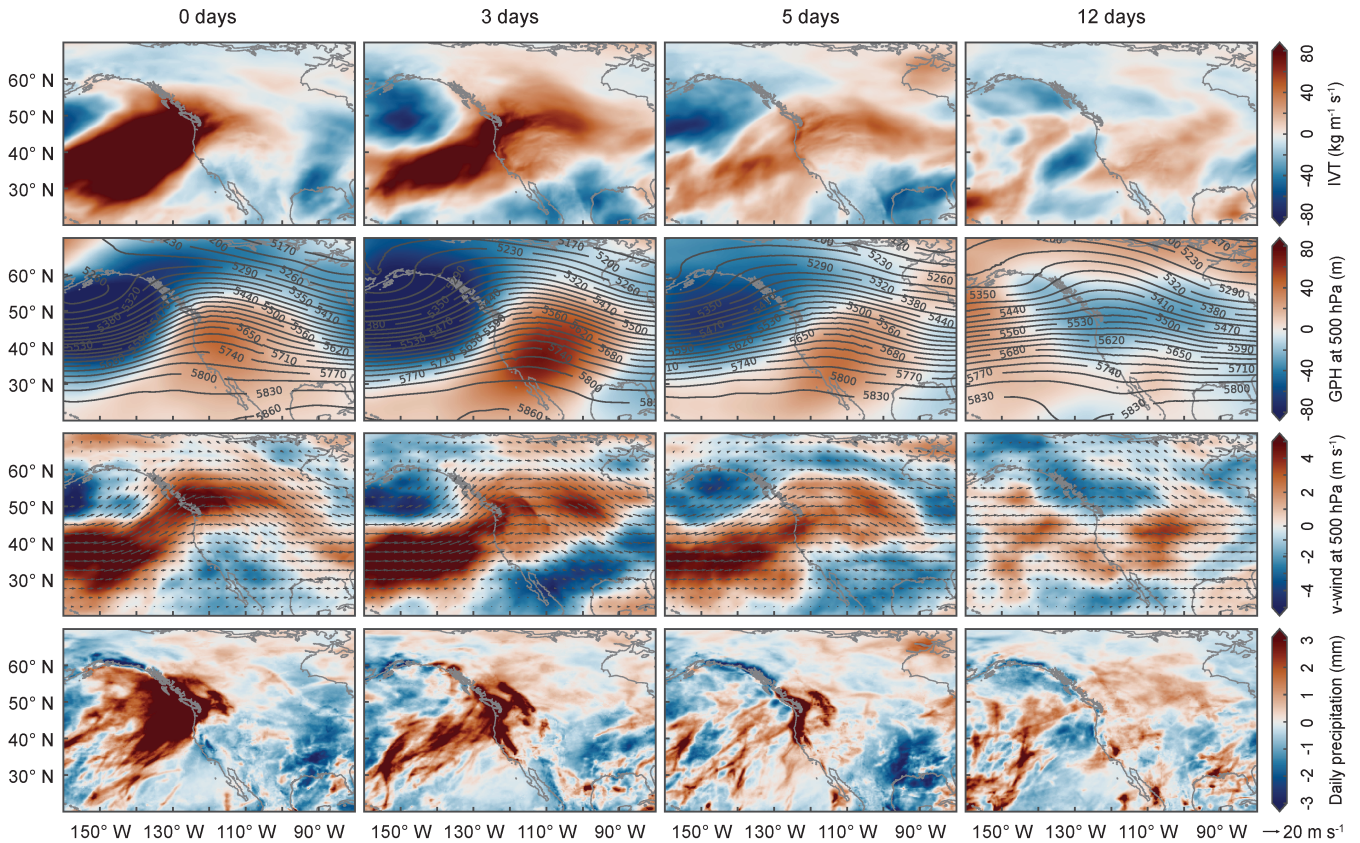


Figure S5. Same as in Fig. 7 but for land-falling ARs that do not synchronize with HPEs in central and eastern Canada.

Northeastern Pacific accompanied by a cold front and a southwesterly steering wind driving the ARs to the western coast of NA. Moreover, on the day of landfall, the mid-level pressure dipole identified in Fig. 7 is present and determines the location of HPEs along the western coast of NA. However, the striking difference between ARs leading to type II events and those leading to type I events is the evolution of this pressure dipole in the days following landfall. Note that the cold front vanishes instead of digging into Canada, preventing the anomalous influx of water vapor from reaching the northern parts of North America, and therefore resulting in the absence of HPEs in central and eastern Canada.

Secondly, in Fig. S6 we present the temporal evolution of the synoptic conditions preceding HPEs in central and eastern Canada that occurred in the absence of land-falling ARs. Note the negative IVT, wind, and precipitation anomalies that are always present over the Northeastern Pacific and the western coast of NA, which are attributable to the warm front located in the northwest of the scene. These specific synoptic conditions are a clear indicator of the absence of land-falling ARs during the 12 precedent days considered for the analysis. For type III events, the climatological drivers are more likely related

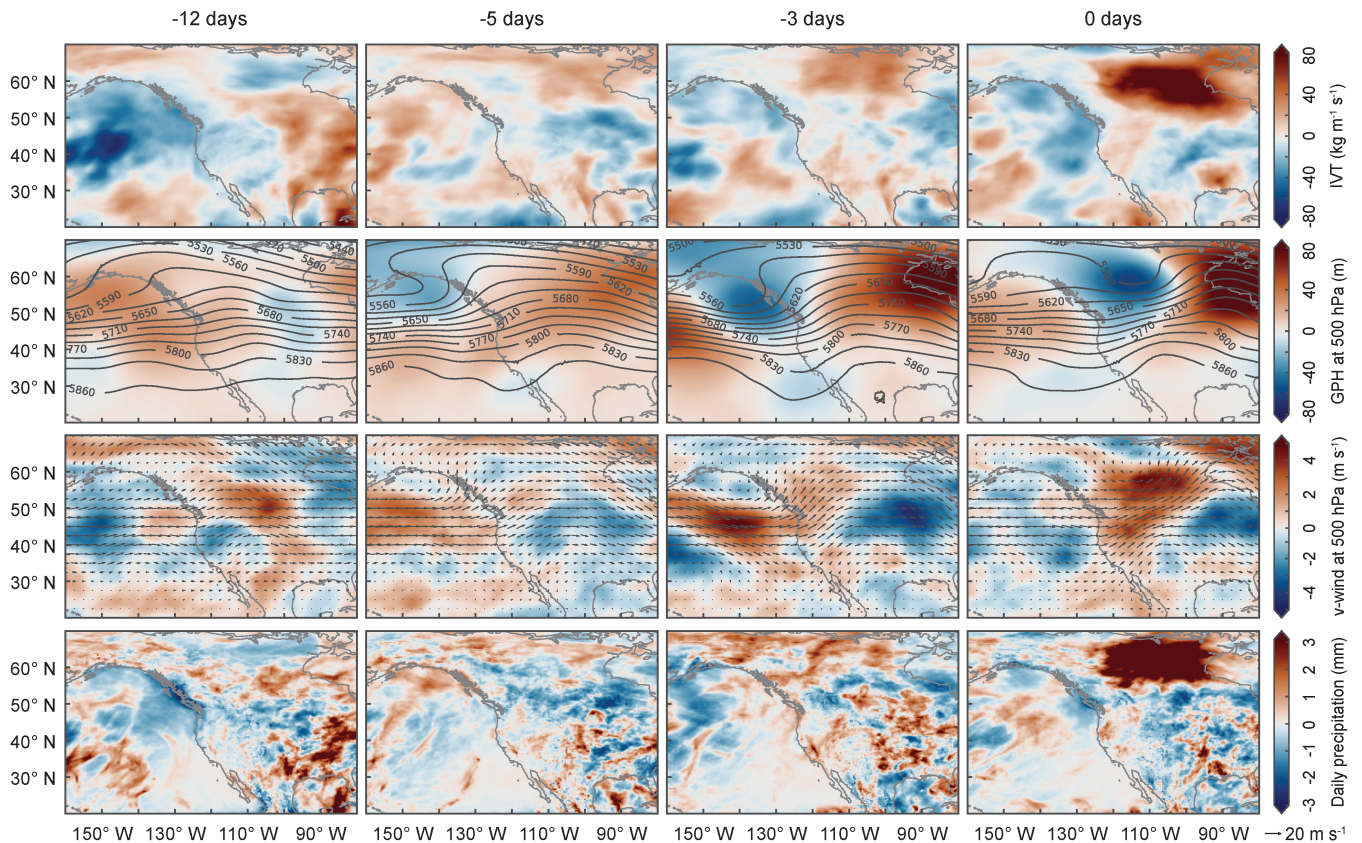


Figure S6. IVT, geopotential height at 500 hPa, wind at 500 hPa, and precipitation anomalies (from top to bottom), from 12, 5, 3, and 0 days (from left to right) before the occurrence of HPEs in central and eastern Canada with no precedent land-falling ARs on the western coast of NA at locations north of 47.5°N, according to the SIO-R1 catalog. Shading, contours and arrows as in Fig. 7

to summertime convective processes forced by the trough located over central Canada when the HPEs occur (right column) (Raddatz and Hanesiak, 2008).

75 S6 Precipitation anomalies for increasing AR levels

As stated in the main manuscript, only considering ARs of level AR4 and higher, or even examining only ARs of level AR5, does not lead to significant correlation between land-falling ARs and HPEs. We suspect that first, the sparsity of the time series does not allow for significant ES scores but also that HPEs do not *only* occur after such strong ARs. To give an argument that these ARs still contribute to the HPEs, we studied the precipitation anomalies in the aftermath of just these exceptional AR events. The results are shown in Fig. S7.

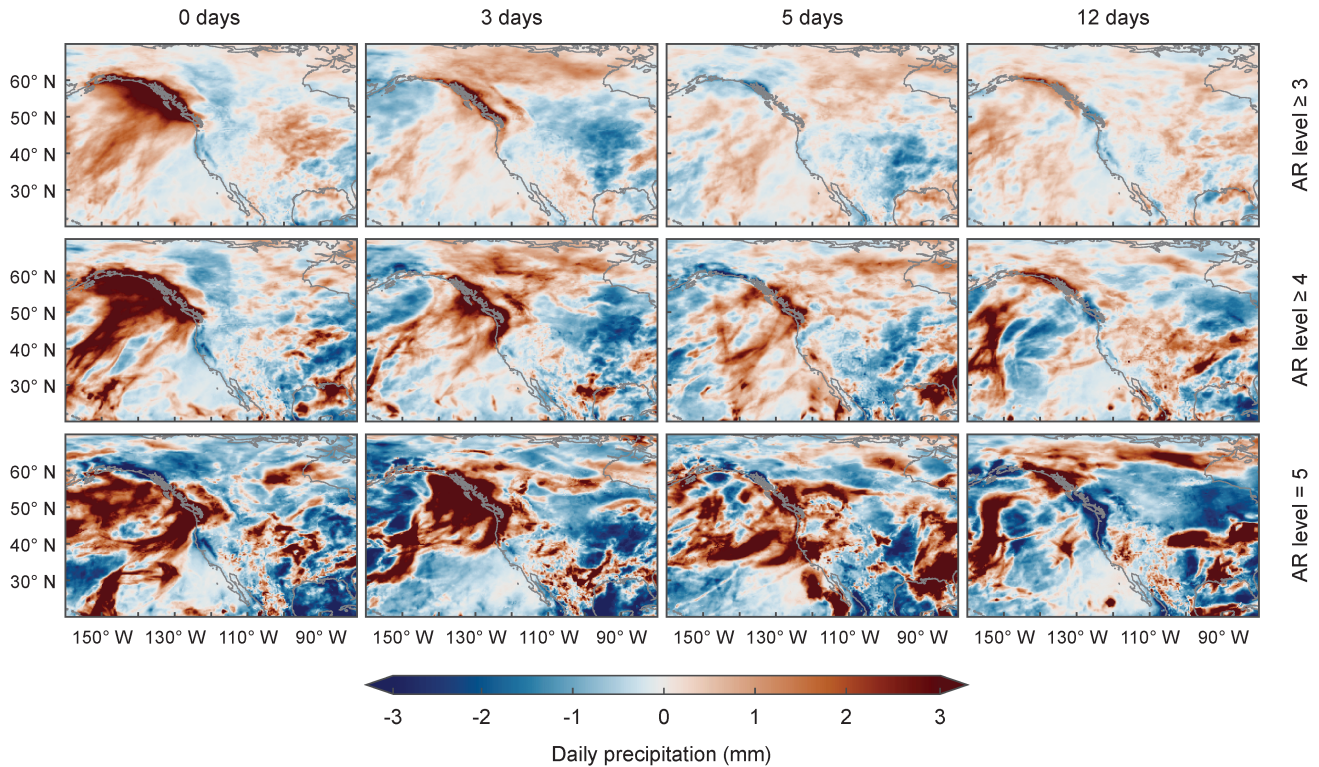


Figure S7. Precipitation anomalies, from 0, 3, 5, and 12 days (from left to right) after the landfall of ARs leading to a delayed synchronization pattern with HPEs in central and eastern Canada. From top to bottom the lower limit of the considered AR level increases. Only ARs with land-falling latitude north of 47.5°N are considered.

The delay grows from left to right and the AR strength increases from top to bottom. As there are only a few events, the pattern differs visibly between the different parameter settings, but nearly all configurations show a considerable signal of above-average precipitation in central and eastern Canada. Therefore, we conclude that these strong AR events are one integral

part of the identified precipitation scheme but explain only one puzzle piece and, thus, do not account just by themselves for
85 the increased precipitation in central and eastern Canada.

References

- Gershunov, A., Shulgina, T., Ralph, F. M., Lavers, D. A., and Rutz, J. J.: Assessing the climate-scale variability of atmospheric rivers affecting western North America, *Geophys. Res. Lett.*, 44, 7900–7908, <https://doi.org/10.1002/2017GL074175>, 2017.
- Neiman, P. J., Ralph, F. M., Wick, G. A., Lundquist, J. D., and Dettinger, M. D.: Meteorological characteristics and overland precipitation impacts of atmospheric rivers affecting the West coast of North America based on eight years of SSM/I satellite observations, *J. Hydrometeorol.*, 9, 22–47, <https://doi.org/10.1175/2007JHM855.1>, 2008.
- O'Brien, T. A., Wehner, M. F., Payne, A. E., Shields, C. A., Rutz, J. J., Leung, L.-R., Ralph, F. M., Collow, A., Gorodetskaya, I., Guan, B., et al.: Increases in future AR count and size: Overview of the ARTMIP Tier 2 CMIP5/6 experiment, *Journal of Geophysical Research: Atmospheres*, 127, e2021JD036013, 2022.
- 95 Raddatz, R. and Hanesiak, J.: Significant summer rainfall in the Canadian Prairie Provinces: modes and mechanisms 2000–2004, *International Journal of Climatology: A Journal of the Royal Meteorological Society*, 28, 1607–1613, 2008.
- Ralph, F. M., Rutz, J. J., Cordeira, J. M., Dettinger, M., Anderson, M., Reynolds, D., Schick, L. J., and Smallcomb, C.: A scale to characterize the strength and impacts of atmospheric rivers, *Bull. Am. Meteorol. Soc.*, 100, 269–289, <https://doi.org/10.1175/BAMS-D-18-0023.1>, 2019.
- 100 Rutz, J. J., Shields, C. A., Lora, J. M., Payne, A. E., Guan, B., Ullrich, P., O'Brien, T., Leung, L. R., Ralph, F. M., Wehner, M., et al.: The atmospheric river tracking method intercomparison project (ARTMIP): quantifying uncertainties in atmospheric river climatology, *Journal of Geophysical Research: Atmospheres*, 124, 13 777–13 802, 2019.
- Shields, C. A., Rutz, J. J., Leung, L.-Y., Ralph, F. M., Wehner, M., Kawzenuk, B., Lora, J. M., McClenny, E., Osborne, T., Payne, A. E., et al.: Atmospheric river tracking method intercomparison project (ARTMIP): project goals and experimental design, *Geoscientific Model Development*, 11, 2455–2474, 2018.
- 105 Traxl, D.: dominiktraxl/artracks: Release v1.0.0, <https://doi.org/10.5281/zenodo.7130642>, 2022.
- Waliser, D. and Guan, B.: Extreme winds and precipitation during landfall of atmospheric rivers, *Nat. Geosci.*, 10, 179–183, <https://doi.org/10.1038/ngeo2894>, 2017.
- Xu, G., Ma, X., and Chang, P.: IPART: A Python Package for Image-Processing based Atmospheric River Tracking, *Journal of Open Source Software*, 5, 2407, <https://doi.org/10.21105/joss.02407>, 2020.
- 110